15—3

Robust and Fast Stereovision Based Road Obstacles Detection for Driving Safety Assistance

Raphael Labayrade and Didier Aubert*
Vehicle-Infrastructure-Driver Interactions Research Unit
LIVIC - INRETS/LCPC

Abstract

This paper deals with a first evaluation of the efficiency and the robustness of the real-time "v-disparity" algorithm in stereovision [1] for generic road obstacles detection towards various types of obstacles (vehicle, pedestrian, motorbike, cyclist, boxes) and under adverse conditions (rain, glowing effect, noise and false matches in the disparity map). The theoretical good properties of the "v-disparity" algorithm - accuracy, robustness, computational speed - are experimentally confirmed. The good results obtained allow us to use this stereo algorithm as the onboard perception process for Driving Safety Assistance : conductor warning and longitudinal control of a low speed automated vehicle (using a second order sliding mode control [2]) in difficult and original situations, at frame rate using no special hardware. Results of experiments - Vehicle following at low speed, Stop'n'Go, Stop on Obstacle (pedestrian, fallen motorbike, load dropping obstacle) - are presented.

1 Introduction

In the context of Driving Safety Assistance, onboard road obstacles detection is an essential task. Stereovision can be used in this purpose, but stereo algorithms are often not robust and fast enough to be used efficiently in the automotive context where meteorologic and lightning conditions are difficult (rain, glowing effect) and where the obstacles detection process must be performed in real time. Nevertheless, the stereo algorithm detailled in [1] (called the "v-disparity" algorithm) presents theoretical good properties to be a generic, robust and real time (using no special hardware) road obstacles detection process. This paper deals with an experimental evaluation of the "v-disparity" algorithm towards various types and under various meteorologic and lighting conditions, and its use for the longitudinal control of an automated vehicle. The paper is organized as follows.

Section 2 presents our experimental protocol. Section 3 summaries the "v-disparity" algorithm, and the method used for robustly detecting generic obstacles. Section 4 evaluates the efficiency of this algorithm for detecting different classes of obstacles and the accuracy of the measurement of the obstacle distance. Section 5 shows the robustness of the method against adverse conditions and its low sensibility to noise and false matches. Lastly, section 6 presents the results of experiments about the longitudinal control of a low speed automated vehicle (based on a second order sliding mode control) using the "v-disparity" algorithm for obstacles detection and distance computation.

*Address: 13 Route de la Miniere, Batiment 140, 78000 Versailles Satory, France. E-mail: raphael.labayrade@lcpc.fr and didier.aubert@inrets.fr

2 Experimental protocol

Fig. 1 presents the stereo sensor used for the experiments (top), the left CCD camera (bottom left), and the configuration area used for the evaluation of the obstacle distance accuracy (bottom right). After configuration, the image planes are parrallel : the epipolar geometry is rectified (epipolar lines correspond to scanning lines in the images of the stereo pair). The parameters of the stereo sensor are $b = 1.03$ m, $h = 1.4$ m, $\theta = 9.75°$, $f = 8.5$ mm, $t_u \approx t_v = 7.2$ μm. The resolution of each image is 380×289 pixels ($\frac{1}{4}PAL$). $Computar^{TM}$ auto-iris lenses and a $Matrox^{TM}$ Meteor II board are used for grabbing images on a PIV 1.4 GHz PC computer running under Microsoft Windows 2000 ©. With this configuration the disparity range investigated is $[0, 150]$ pixels.

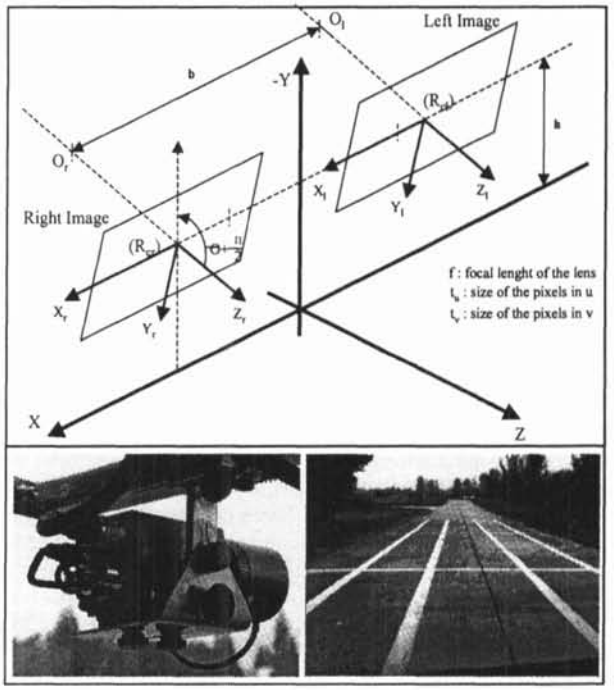

Figure 1: Stereo sensor (top). Left camera (bottom left). Configuration area (bottom right).

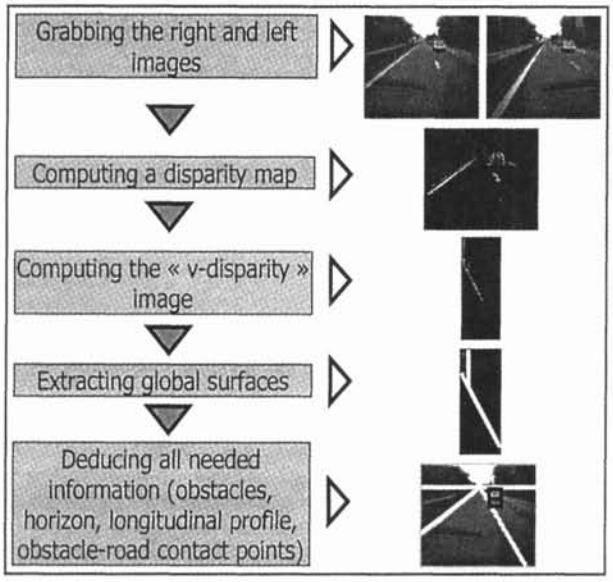

Figure 2: Framework (left) and exemple of implementation (right) of the "v-disparity" algorithm.

3 The "v-disparity" algorithm

The "v-disparity" algorithm is described in details in [1]. A framework for our obstacles detection process is presented in Fig. 2 (left). Our current implementation of this framework is as follows (see Fig. 2 (right)). First, non-horizontal edges are extracted from the two images of the stereo pair and matched (using normalized correlation) in order to obtain a sparse disparity map. Then, disparity is accumulated along scanning lines in order to obtain the "v-disparity" grey image (see also Fig. 8 (top)). In the "v-disparity" image, scene plane of interest with equation $Z = aY + d$ is projected along the following straigh line [1]:

$$\Delta = \frac{b}{ah - d}((v - v_0)(a\cos\theta + \sin\theta) + \alpha(a\sin\theta - \cos\theta)) \quad (1)$$

where Δ is the disparity, v is the ordinate of a pixel in the image coordinate system, v_0 is the ordinate of the center of the image, and $\alpha = \frac{f}{t_u} \approx \frac{f}{t_v}$.

The road is characterised as a set of planes and obstacles are characterised as vertical planes. Thus, extracting straight lines in the "v-disparity" image leads to extract road surface and obstacles. All needed information for performing generic obstacles detection is then deduced : longitudinal profile of the road surface (not necessary planar), horizon line location, obstacle-road contact point.

4 Detection of various types of obstacles

Six types of obstacles (see Fig. 3) are used for the evaluation of the distance computation accuracy and for the confidence value computation : a 1.90m high pedestrian, a 1.75m high cyclist, a 1.50m high vehicle, a fallen motorbike, a $0.7 \times 0.7 \times 0.4m$ box, and a $0.3 \times 0.3 \times 0.2m$ box. Every obstacle is positioned along the

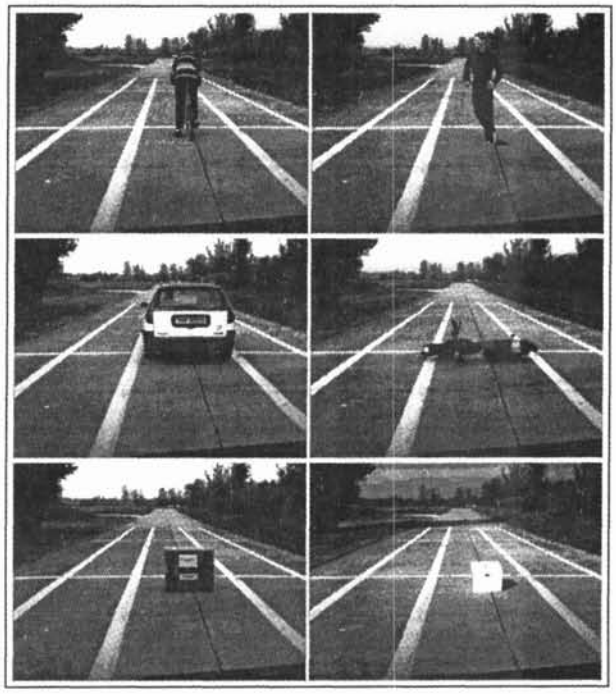

Figure 3: The six obstacles used for evaluation of distance computation accuracy, located at 10 meters from the vehicle (see text).

axis of the vehicle, at the following distances : 3m, 5m, 10m, 15m, 20m, 25m, 30m, 35m, 40m. The weather is cloudy.

For each obstacle at every distance, the "v-disparity" image is computed, the obstacle (characterised by a vertical plane) is detected, the road surface is evaluated and the road-obstacle contact point is computed. The distance D between the vehicle and the obstacle is given by :

$$D = \frac{b(\alpha\cos\theta - (v_r - v_0)\sin\theta)}{\Delta} \quad (2)$$

where v_r is the ordinate of the road-obstacle contact point in the image.

Fig. 4 and 5 show the distance computation results. Since the disparity precision is currently one pixel, the two theoretical curves that define the theoretical range (upper and lower) of the distance evaluation are drawn on the figure. The difference between the reference distance and the computed one is 0.7% at $3m$ and 14% at $40m$. It shoud be noticed that the actual computed distance values are mostly in the theoretical range. The out-of-range values concern distances less than $20m$, where the plane characterisation of the obstacles is not precise enough. However, the error between the reference distance and the computed distance does not exceed 7%. Others stereo systems has been experimentaly evaluted in [3], [4] and [5].

The confidence value is computed by adding all the "v-disparity" grey values for pixels belonging to the same obstacle. In order to avoid any false detection, an obstacle is considered to be detected only if the confidence value is above a threshold set to 20 in our system.

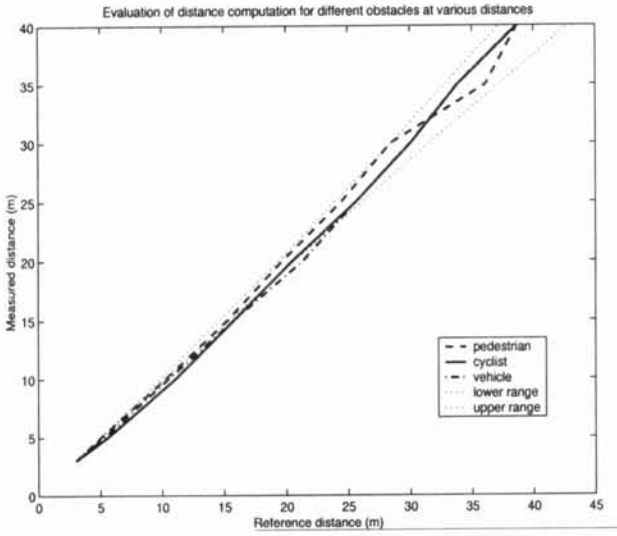

Figure 4: Distance computation accuracy.

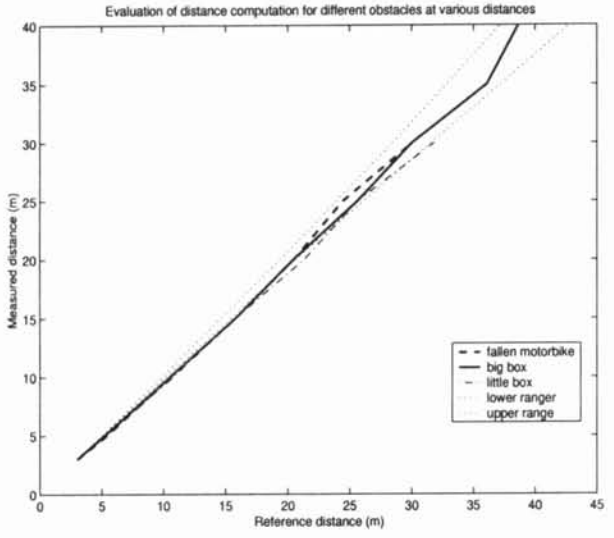

Figure 5: Distance computation accuracy.

Fig. 6 shows the confidence value results for all the obstacles. This confidence value increases the higher is the obstacle, when the obstacles distance decreases, and when the number of non-vertical edges of the obstacles increases. It should be noticed that the confidence value of the little box and the motorbike is under 20 when the distance is above 30m. This is mainly because the heigh of these obstacles is low.

5 Detection under adverse conditions

The system has been tested intensively under various and adverse meterologic conditions (glowing effects due to sun, rain). Experiments shows that the system is merely affected by such conditions until the obstacle is visible. Fig. 7 shows examples of detection under adverse conditions. In both cases the obstacle (a vehicle) is perfectly detected.

Moreover, experiments of gaussian noise addition and good matches removal (replaced by randomized false matches) in the disparity map show that the "v-disparity" algorithm goes on working efficiently even

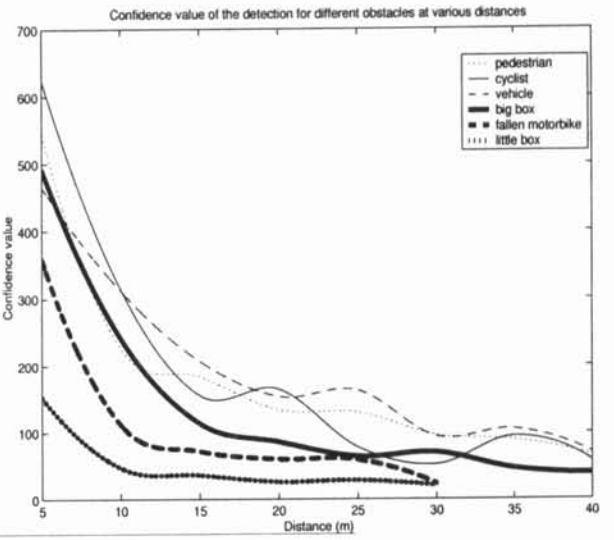

Figure 6: Confidence value.

when there is 96% noise addition or 80% good matches removal (see Fig. 8. top : the reference disparity map and corresponding "v-disparity" image - middle : 96% gaussian noise addition - bottom : 80% good matches removal) for a vehicle located at $20m$. In both cases, relevant information can still be extracted and the obstacle detection process is efficient. These experiments do not represent perfectly the real noise that can affect the disparity map (which is more likely to be correlated noise) but gives an idea about the robustness of the algorithm.

For all the experiments, the tests and the evaluations carried out, computation time does not exceed 40 ms.

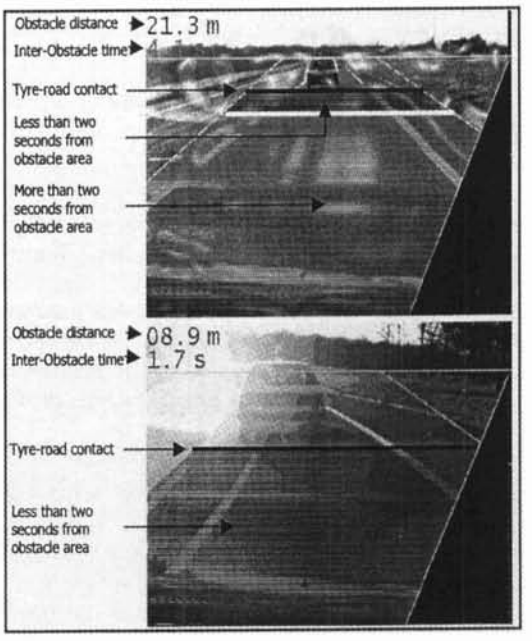

Figure 7: Detection of obstacle under rainy (top) and glowing (bottom) conditions.

6 Longitudinal control of a low speed automated vehicle

The algorithm has been implemented onboard and first tested as a warning system to inform the driver that an obstacle was located at less than 2 seconds from his vehicle : a warning area was drawn on the road image (see Fig. 7). The algorithm has then been combined with a control module in order to perform automated longitudinal control at low speed automated (based on a second order sliding mode control). Various and difficult situations of Driving Safety Assistance has been tested : Vehicle Following at Low Speed, Stop'n'Go, Stop on Obstacles (pedestrian, fallen motorbike, load dropping obstacle). Figs. 9, 10 and 11 show the results of Vehicle Following at Low Speed, Stop'n'Go, Stop on pedestrian. Results regarding Stop on fallen motorbike and Stop on load dropping obstacle are similar to the ones shown in Fig. 11. As we can see on the curves, the desired interdistance and the measured interdistance are close to each other.

7 Conclusion

This paper has presented a first evaluation and experimental results that confirm the theoretical good properties of the "v-disparity" algorithm [1]. Distance computation accuracy and confidence have been evaluated. Moreover, the presented experiments show that stereovision can be used as a robust perception process for various situations of Driver Safety Assistance at frame rate using no special hardware. Tests of emergency braking and collision avoidance at higher speed will be carried out soon. Future work will also be concerned with the evaluation of the system in night conditions.

8 Acknowledgments

The authors would like to acknowledge Pr. Jean Devars's contribution (University of Paris VI). This work is partly founded by the European CARSENSE project and the french MICADO project.

References

[1] R. Labayrade, D. Aubert, J. P. Tarel, "Real Time Obstacle Detection on Non Flat Road Geometry through V-Disparity Representation", IEEE Intelligent Vehicules Symposium, Versailles, June 2002.

[2] L. Nouveliere, S. Mammar, J. Sainte-Marie, "Longitudinal control of low speed automated vehicles using a second order sliding mode control", IEEE Intelligent Vehicles Symposium, Tokyo, May 2001.

[3] M. Bertozzi, A. Broggi - "GOLD: A parallel real-time stereo vision system for generic obstacle and lane detection", IEEE Transaction on image processing, Vol. 7, N1, January 1998.

[4] T.A. Williamson - "A high-performance stereo vision system for obstacle detection ", Phd, Carnegie Mellon University, September 1998.

[5] G. Toulminet, A. Bensrhair, S. Mousset, A. Broggi, P. Mich, "Systeme de stereovision pour la detection d'obstacles et de vehicule temps reel". In Procs. 18th Symposium GRETSI'01 on Signal and Image Processing, Toulouse, France, September 2001.

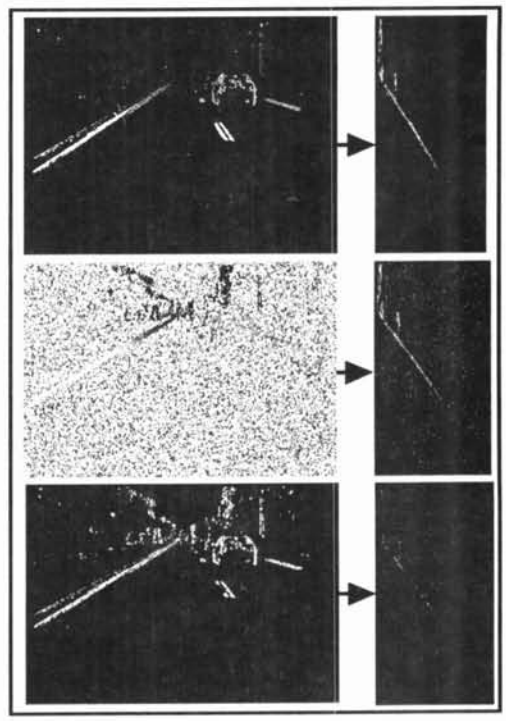

Figure 8: Robustness towards gaussian noise and false matches in the disparity map (see text). Relevant information can still be extracted.

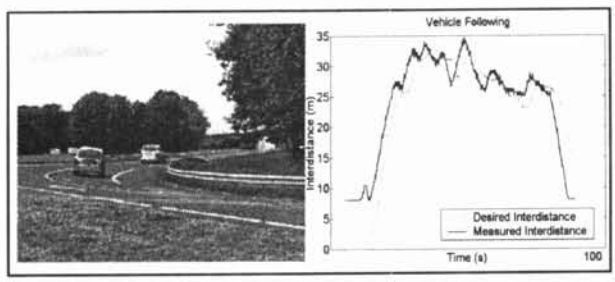

Figure 9: Vehicle Following: comparison between measured and desired interdistance.

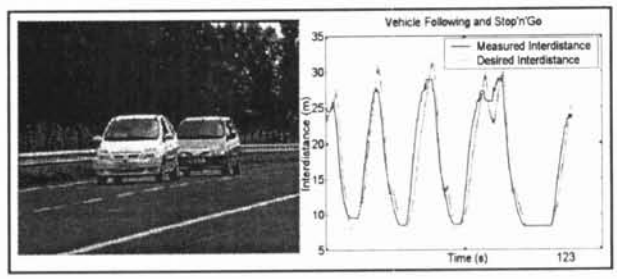

Figure 10: Stop'n'Go: comparison between measured and desired interdistance.

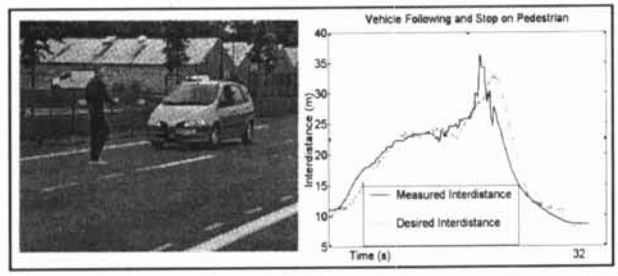

Figure 11: Stop on pedestrian: comparison between measured and desired interdistance.